figure shows that ε_f increases linearly with hydrostatic pressure for pressures up to approximately 300 MPa but increases much less rapidly at pressures above this.

When longitudinal sections of the specimens fractured at the pressures shown in Fig. 1 were examined the number and distribution of voids in the necked region was found to be strongly pressure dependent. Figure 2 shows SEM micrographs of regions near the fracture surfaces of specimens fractured at 0.1 and 500 MPa. The lighter regions in these micrographs represent lead inclusions, and the voids, which are black, can be seen to be associated with these. Table 1 gives the approximate numbers of voids visible at a magnification of $\times 500$ and the distances from the fracture surfaces to which void formation extended, for a series of specimens fractured at pressures of 0.1, 300, 400 and 550 MPa. This shows that the specimens fractured at 0.1 and 300 MPa contained many voids, which occurred in a zone about 1 mm deep beneath the fracture surface. The specimens fractured at 400 and 550 MPa however contained only a few visible voids, which were confined to a small distance beneath the fracture surface. The conditions under which void formation was restricted therefore appear to correspond to those which produced the reduction in slope of the curve in Fig. 1.

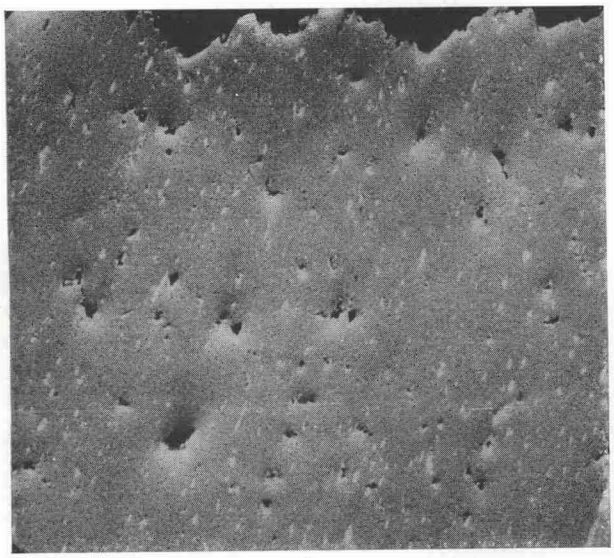

(a)

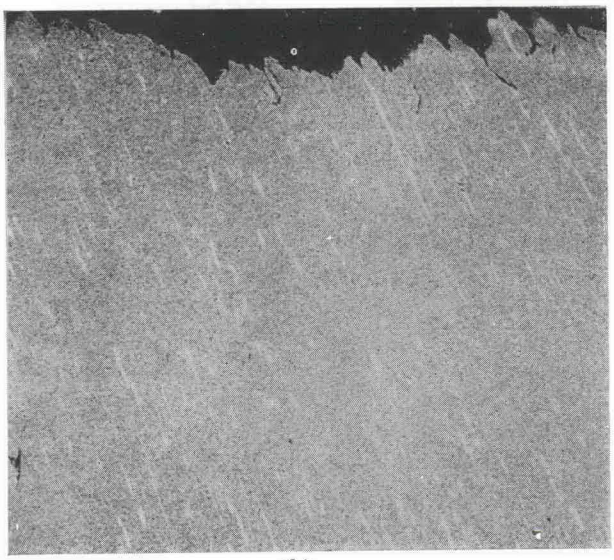

(b)

FIG. 2. Scanning electron micrographs of longitudinal sections of regions near the fracture surfaces of specimens fractured at (a) 0.1 MPa and (b) 550 MPa. $\times 200$.

TABLE 1.

Hydrostatic pressure (MPa)	Total number of voids (Approx)	Maximum distance voids from fracture (mm)
0.1	100	1.3
300	40	0.7
400	15	0.2
550	10	0.1

SEM examination of the fracture surfaces of specimens fractured at all pressures showed that these surfaces were made up of two distinct regions: a central region of rough appearance as shown in Fig. 3(a), and an outer region of smoother appearance as shown in Fig. 3(b). The appearances of the surfaces of these regions were similar for all pressures. The structure of the central region is usually attributed to void coalescence while that of the outer region is attributed to shear tearing.[10] The principal effect of pressure on the fracture surfaces was in the area occupied by the central region. This area decreased considerably as the pressure of the test was increased from atmospheric pressure to 300 MPa but above 300 MPa the area remained approximately constant.

(b) *Series II*

(i) *Tests at* 200 *MPa.* Specimens were strained to a number of points on the load–extension curve. Measurements of the minimum neck radius (r), the radius of curvature of the contour of the neck (R) and the final load for each specimen are given in Table 2. When longitudinal sections of the specimens were examined it was found that visible voids were present only in the specimen taken to the highest strain (ε value of 1.0).

(ii) *Tests at* 500 *MPa.* Specimens were again strained to a number of points on the load-extension curve and Table 2 gives the value of r, R and load obtained. Examination of longitudinal sections of the

(a)

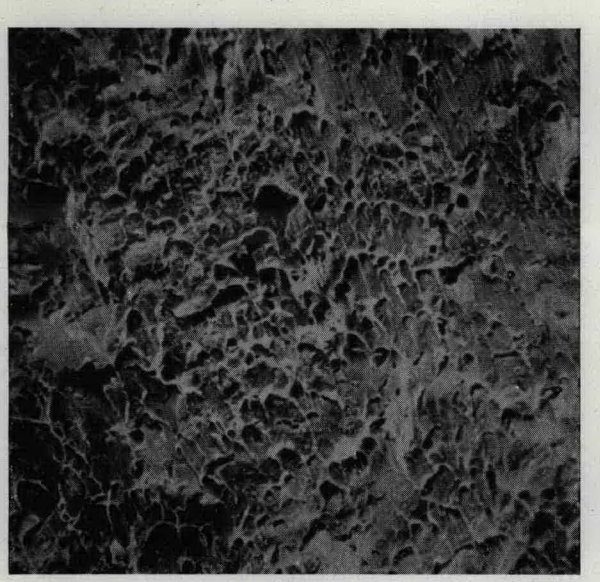

(b)

FIG. 3. Scanning electron micrographs of (a) the central region and (b) the outer region of the fractured surface of a specimen fractured in tension. ×560.

necked regions of these specimens revealed that very little visible void formation had occurred up to the highest strains obtained.

The stress system at the centre of the neck of a specimen undergoing tensile deformation whilst subjected to an external hydrostatic pressure can be calculated using the equations derived by Bridgman.[4] Bridgman showed that the stress system is made up of a hydrostatic or triaxial component H plus a longitudinal tensile component T. These components being approximately given by

$$H = -P + F \ln \frac{r^2 + 2rR}{2rR} \tag{2}$$

and

$$T = F, \tag{3}$$

where

$$F = \frac{1}{(1 + 2R/r) \ln (1 + \frac{1}{2}r/R)} \frac{\text{Load}}{\pi r^2}$$

and P is hydrostatic pressure. These equations were used to find the resultant triaxial and tensile stress components in each of the specimens tested at 200 and 500 MPa. The results of these calculations are shown in Table 2 together with the natural strain for each specimen. The calculated H values for the tests at both pressures are plotted against natural strain in Fig. 4. These curves show that the resultant triaxial components of stress eventually become positive (tensile) for tests at both pressures. The values of natural strain at which these stresses become tensile increases markedly with pressure however. It should be noted that equations (2) and (3) refer only to the point at the centre of the minimum diameter of the neck. Since this is the point of maximum triaxial stress component this stress will decrease with distance from this point. Also, the equations assume a homogeneous material and are therefore not strictly applicable if a significant number of voids are present.

TABLE 2.

Pressure MPa	r (mm)	R (mm)	Load (Kg)	ε	H MPa	T MPa
200	1.63	44.0	513	0.41	−178	1175
200	1.50	14.7	506	0.58	−135	1306
200	1.43	7.3	463	0.67	−84	1239
200	1.39	5.7	481	0.73	−47	1325
200	1.23	1.78	388	0.95	+124	1104
500	1.61	31.0	525	0.43	−469	1218
500	1.51	20.4	494	0.56	−453	1281
500	1.45	5.6	481	0.64	−353	1207
500	1.24	3.05	400	0.95	−268	1271
500	1.14	2.34	375	1.13	−201	1349
500	0.975	0.81	312	1.44	+58	1169